Chemical Engineering Journal 162 (2010) 1082–1090

Contents lists available at ScienceDirect

Chemical Engineering Journal

journal homepage: www.elsevier.com/locate/cej

AISI 304 austenitic stainless steel monoliths: Modification of the oxidation layer and catalytic coatings after deposition and its catalytic implications

L.M. Martínez T*, O. Sanz, M.A. Centeno, J.A. Odriozola

Instituto de Ciencia de Materiales de Sevilla CSIC, Universidad de Sevilla, Avda, Américo Vespucio 49, 41092 Sevilla, Spain

ARTICLE INFO

Article history:
Received 4 March 2010
Received in revised form 1 July 2010
Accepted 2 July 2010

Keywords:
Metallic monolith
Austenitic stainless steel
Gold catalysts
CO oxidation

ABSTRACT

Monolithic CeO_2 and Au/CeO_2 catalysts were prepared using austenitic stainless steel (AISI 304) as metallic substrate. Both monolithic and powdered catalysts were characterized before and after CO oxidation reaction by N_2 adsorption–desorption, XRD, SEM, TEM and GD-OES. Catalyst deposition on the stainless steel surface results in modifications of the catalyst, the oxide scale and the oxide scale/alloy interface through the interaction between the coating and the steel oxidation layer. Besides this, oxidation of the alloy is also detected. The extension and nature of these modifications depends on the catalyst nature, and on the reaction conditions. As a result of these modifications CO oxidation on Au/CeO_2 catalysts is enhanced and gold surface dynamics is modified.

1. Introduction

During the last decades a growing interest in structured catalysts and reactors has developed, among these are monolithic catalysts. These are continuous unitary structures containing many narrow parallel channels [1,2]. These are a valuable alternative to conventional fixed beds and slurry catalytic reactors eliminating most of the drawbacks associated to these. Catalytically active ingredients are dispersed uniformly over the metallic or ceramic monolithic. Metallic monoliths show some advantages over ceramic ones such as higher thermal conductivity, lower heat capacities and greater thermal and mechanical shock resistance [2]. Moreover, they can be made with thinner walls than their ceramic counterparts, resulting in a lower pressure drop for the same cell density and a higher contact surface area per unit of volume, which provides more effective conversion. The most popular method to coat monolithic structures is washcoating. The ultimate goal of the process is to load the monolith with a certain amount a layer of the catalytically active phase homogeneously dispersed and strongly adhered onto the monolith walls. However, the nonporous nature of metal substrates together with thermal expansion mismatch between the metal and the washcoat results in lack of adherence during thermal cycling. Therefore, coating of metallic monoliths is more complex than coating of ceramic ones. For improving adherence a suitable thermal treatment of the metallic surface is required. We have already carried out an extensive study of the oxidation layer (oxide scale) formed on austenitic stainless steel (AISI 304) monoliths upon thermal treatment [3,4] and used, this alloy, as an alternative to conventional Al-alloyed ferritic stainless steel monoliths [2,5,6] to deposit catalysts. Thermal treatment of the AISI 304 monolith in synthetic air at 900 °C for 1 h oxidizes the alloy surface in a controlled way generating an adherent, rough, thermal and mechanically resistant oxide layer, which results appropriate to adhere catalysts.

However, the nature of the oxide layer may affect the monolith catalytic properties, since the alloy scale elements could present catalytic properties by themselves [7] or act as dopants of the deposited catalytic layer. On the other hand, the physico-chemical properties of the scale might be affected by the presence of the so-called reactive elements (REE), i.e. cerium, in the catalytic layer. It has been evidenced that cerium deposited on stainless steels surfaces migrates to the alloy/scale interface affecting the characteristics and properties of the oxide scale layer [8–10] whatever the deposition method: pyrolysis of aerosols, ion implantation, immersion in cerium nitrate or sol–gel oxide precursor solutions [8,11–13].

In this work we try to elucidate the modifications of both the catalyst and the oxidation layer when coating on a metallic substrate is done. These changes may affect the activity and selectivity of the catalytic devices. Moreover, progress of these modifications may occur under reaction conditions altering catalytic properties upon time. CeO_2 and Au/CeO_2 based catalysts are used as model systems in this study. Gold-based catalysts are known by their high activity towards oxidation reactions, especially CO oxidation at low temperature [14–21]. In these catalysts, the influence of the nature of the support and the gold particle size has been described as key factors for the activity of the systems. However, the nature of the active site (gold oxidation state) and its modification along the course of

* Corresponding author.
E-mail address: leidy@icmse.csic.es (L.M. Martínez T).

1385-8947/$ – see front matter © 2010 Elsevier B.V. All rights reserved.
doi:10.1016/j.cej.2010.07.005

Table 1
Composition of the commercial EN-1.4301 austenitic stainless steel (Fe balance).

Element (wt.%)	Cr	Si	C	Mn	Cu	Ni	N	Mo	P	S	Co	V	W
AISI 304	18.4	0.44	0.064	1.45	0.23	8.11	0.057	0.25	0.03	0.001	0.2	0.13	0.15

the reaction are still under discussion. In the case of gold-based structured catalysts (monoliths and/or microreactors) no studies concerning to the possible modification of the catalytic layer due to the interaction of the metallic substrate and the catalytic deposit has been published to the best of our knowledge.

Using the catalytic CO oxidation as a test reaction the role of the catalyst-oxidation layer of the metallic substrate interaction is studied. It is demonstrated that stainless steel coated Au/CeO_2 catalysts stand comparison with the powdered ones. The modification induced by the metallic elements present on the oxide scale enhances the activity of the catalyst and the surface dynamics of Au/CeO_2 catalysts.

2. Experimental

2.1. Preparation of the structured support

The metallic substrates were commercial EN-1.4301 austenitic stainless steel sheets (Goodfellow, 50 μm thick) with the composition shown in Table 1.

Before the pretreatment, 24 cm × 3 cm foils were cleaned with water and soap, thoroughly rinsed with water and acetone, and finally dried at room temperature. Before any further treatment the metallic foils stand in air for 24 h for passivation. Monoliths were manufactured by rolling up corrugated and flat foils around a spindle. The final monoliths are cylinders 30 mm height and 16 mm diameter, with 240 cm^2 geometric surface area and a cell density of 55 cell/cm^2. These monoliths were submitted to a thermal treatment (900 °C, 60 min) in 10 ml min^{-1} flow of synthetic air (Air Liquide, 99.999 pure, <3 ppm H_2O) to create an oxide scale on the base alloy with the adequate physical parameters (roughness, homogeneity and adherence) for anchoring the washcoated catalysts [3,22].

2.2. Catalyst coating deposition

Colloidal solutions with 10 wt.% solids content were prepared by adding the adequate amount of distilled water to a commercial CeO_2 colloid (Nyacol CeO_2 ACT) to deposit the catalytic ceria layer on the structured support [3]. Commercial ceria colloid contains 20 wt.% CeO_2 and acetate as counter ion (0.4 mol/mol) [3]. The adequate amount of the metallic gold precursor (gold acetate, Alfa Aesar 99.99% pure) to obtain a 1 wt.% gold concentration in the final solid was mixed with the colloidal dispersion in the absence of light for preparing Au/CeO_2 catalysts [4,23]. Gold acetate is used instead of the popular chloroauric acid as gold source since chloride ions attack the stainless steel surface causing pitting [17,24] and it is sufficiently soluble in the solution based on colloidal ceria acetate. The prepared colloidal dispersions had a viscosity of 3.0 cp and a final pH of 3.0. This low pH is far away from CeO_2 particles IEP, which was measured to be 7.0, ensuring the stability of the colloids during the deposition procedure.

The oxidized monoliths were immersed into the colloidal dispersion for 1 min and then withdrawn at 3 cm h^{-1} constant rate. To avoid the obstruction of the channels of the monolith, the colloid excess was removed by centrifugation at 400 rpm for 10 min. After that, the monoliths were dried by freeze-drying for 4 h and finally, calcined at 300 °C for 4 h with a heating ramp of 2 °C min^{-1}. This drying and calcination procedure has been shown as optimal for avoiding crack phenomena and obtaining a homogeneous and well-adhered catalytic layer [3,25]. The amount of washcoated catalyst was measured weighting the monolith before and after the coating procedure. Three successive coating, drying and calcination cycles were repeated until ~100 mg of loaded catalyst was achieved.

2.3. Powder catalysts

Powder catalysts were obtained by drying at 80 °C and further calcining for 4 h at 300 °C the corresponding colloidal dispersions.

2.4. Characterization techniques

X-ray diffraction (XRD) analysis was performed on a D500 Siemens diffractometer. Diffraction patterns were recorded using Cu Kα radiation (λ = 1.5404 Å) over a 20–80° 2θ-range using a position-sensitive detector with 0.05° step size at a scan rate of 1° min^{-1}.

The textural properties were studied by N_2 adsorption–desorption isotherms at liquid nitrogen temperature in a Micromeritics ASAP 2020 apparatus between 0.1 and 0.995 relative pressure using a homemade cell that allows analyzing the complete monolith. Before analysis, the monoliths were degassed for 2 h at 150 °C in vacuum. Pore size distribution was calculated using the BJH method.

Scanning electron microscopy (SEM) observations were carried out in a JEOL 5400 microscope. SEM analyzed cross-sections of the pre-treated monoliths. Before analysis monolith cross-sections were Pt coated in a Sputter Coater TELSTAR EMITECH K-550 and then a thick Ni layer was electrolytically grown in order to protect the catalytic layer/oxide scale during grounding and polishing.

The ultrasonic method was selected to evaluate the adherence of the catalytic layer to the metallic substrate [3,26]. The monoliths were immersed in acetone and then submitted to an ultrasonic treatment in a Cole Parmer ultrasonic bath (47 kHz and 130 W) for 60 min at room temperature. After that, the samples were dried and calcined. The mass difference of the sample before and after the ultrasonic test was used to measure the adherence. The adherence is defined as the ratio of retained amount of the catalytic layer to the amount of the deposited catalytic layer expressed as percentage.

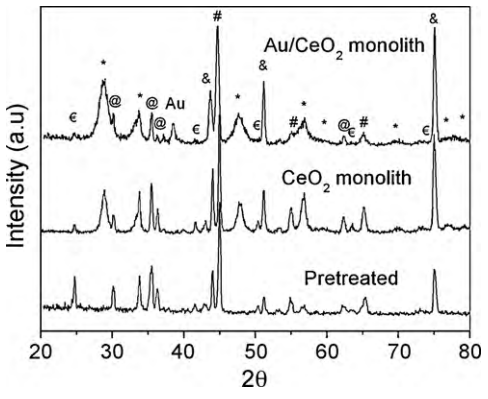

Fig. 1. XRD of monolithic catalytic devices. Symbols: (*) CeO_2, (∈) Cr_2O_3, (@) $Mn_{1+x}Cr_{2-x}O_{4-x}$, (&) austenite, (#) martensite and (Au) gold.

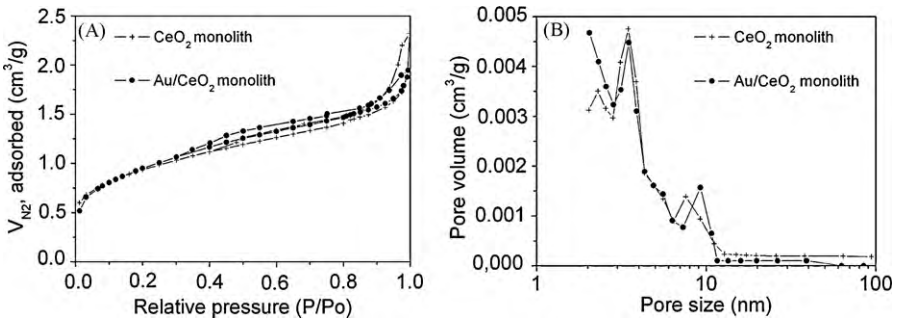

Fig. 2. (A) N_2 adsorption–desorption isotherms and (B) pore size distribution of coated monoliths.

Roughness was measured with a Mitutoyo SJ-201P surface roughness tester.

In-depth compositional analysis of both the oxide scale and the catalytic layer were determined by Glow Discharge Optical Emission Spectroscopy (GD-OES) experiments using a LECO GDS 750A spectrometer. The GD-OES analyses were performed with a Grimm lamp in the DC mode at 700 V using a constant power of 14 W. In every case a 4 mm area was analyzed ensuring average macroscopic information of the analyzed layers.

Inductively coupled plasma optical emission spectroscopy (ICP-OES) using a Perkin-Elmer Optima 3000DV ICP spectrometer was used for measuring gold loading in the deposited catalyst. The gold amount present in the colloidal dispersion before and after the washcoating process is used for calculating gold loading in the monolithic device. X-ray fluorescence spectrometry (XRF) using a Siemens SRS 3000 sequential spectrophotometer with a rhodium tube as the source of radiation was used for determining gold content of powdered catalysts. XRF measurements were performed onto pressed pellets (sample included in 10 wt.% of wax).

Transmission electron microscopy (TEM) observations were carried out in a Philips CM200 microscope working at 200 kV. The samples were dispersed in ethanol by sonication and dropped on a copper grid coated with a carbon film.

2.5. Activity measurements

Carbon monoxide oxidation reaction was carried out in a conventional continuous flow U-shaped glass reactor working at atmospheric pressure. The composition of the inlet and outlet gases was analyzed with a Balzers Omnistar Bentchtop mass spectrometer with capabilities for quantitative analysis. The light-off curves of CO oxidation (300 °C, 5 °C min^{-1}) were obtained with a gas mixture containing 3.4% CO and 21% O_2 balanced by He at a total flow rate of 42 ml min^{-1}. Empty reactor (without sample) shows no activity under these conditions. For best comparing powdered and monolithic catalysts the mass of catalyst and volume of the catalytic bed was kept the same. Catalytic tests using powered catalysts were carried out using a 6 cm^3 crushed glass beads (~200–400 μm) in which ~100 mg of catalysts was diluted. Both monoliths and powders were pre-activated "in situ" at 300 °C for 60 min with 21% O_2 in He at a flow of 30 ml min^{-1} and then stabilized at room temperature before the light-off curved started.

3. Results

3.1. Structured supports

Upon thermal treatment in synthetic air flow at 900 °C for 60 min a homogeneous and well-adhered oxide layer is formed over the stainless steel surface. Our group has already reported a complete characterization of such oxide layer [3–5]. This is mainly composed of Cr_2O_3 and $Mn_{1+x}Cr_{2-x}O_{4-x}$ spinel-type compounds with irregular shaped crystals and sizes ranging from 0.1 to 0.5 μm [3,22,25]. $Mn_{1+x}Cr_{2-x}O_{4-x}$ is generated in the outermost part of the scale and Cr_2O_3 remains in the innermost one. The thickness of this oxide scale was estimated from the cross-section of the monolith in SEM micrographs to be 0.65 μm. In-depth profile composition of the oxide scale measure by GD-OES showed a structured sequence of layers.[1] The GD-OES measured total scale thickness was ca. 0.7 μm in close agreement with SEM results. The scale is composed of a 0.24 μm thick outer layer where Cr and Mn oxides are the dominant species, although it is enriched in iron species in the outermost surface. Underneath this layer, the oxide scale is mainly chromium oxide [3,22]. At the scale–alloy interface a phase mostly composed of silicon and oxygen is detected. Due to the formation of the oxide layer after heating, the roughness of the metallic surface increases from 0.5 to 1.3–1.4 μm. BET surface area of pre-treated AISI 304 steel monoliths is lower than 1 m^2 $monolith^{-1}$.

3.2. Monolithic catalytic devices

The ICP-OES analyses of the colloidal dispersions after the deposition procedure only indicate the presence of gold and cerium species, ruling out lixiviation of metallic elements from the metallic surface. Gold loading is measured to be 0.84 wt.% Au quite close to the target value of 1.0 wt.%.

XRD patterns of the ceria-deposited monolithic devices show besides the characteristics peaks of the pre-treated metallic surface, diffraction lines corresponding to CeO_2 (cerianite, JCPDS = 34-0394), Fig. 1. An additional diffraction line at $2\theta = 38.1°$ is observed for Au/CeO_2 catalysts deposited on stainless steel monoliths, this line being characteristic of the (2 0 0) plane of metallic gold (JCPDS = 4-0784). Scherrer equation has been used to estimate the average crystalline domain size of the prepared catalysts; ceria crystal sizes are calculated to be 12 and 7 nm for ceria and gold/ceria monoliths, respectively. The average crystal size of gold particles in gold/ceria monoliths was estimated in 21 nm.

The main surface characteristics of the prepared monolithic catalysts coated by CeO_2 and Au/CeO_2 obtained from N_2 absorption–desorption isotherms (Fig. 2) are shown in Table 2. The isotherms correspond to typical mesoporous materials having average pore radius of 41 and 53 Å for CeO_2 and Au/CeO_2 catalysts, respectively. BET areas of the complete monoliths are 10 and 13 m^2 for ceria and gold/ceria ones. An estimate of the surface area and pore volume considering just the catalyst loadings results in 100 m^2/g ($V_p = 0.130$ cm^3/g) and 121 m^2/g ($V_p = 0.113$ cm^3/g) for CeO_2 and Au/CeO_2 catalysts, respectively. The catalyst adherence was excellent (~99%) in both monoliths. The theoretical average

[1] Top view and cross-section SEM images as well as GD-OES results of the oxidized stainless steel surface can be found elsewhere [3].

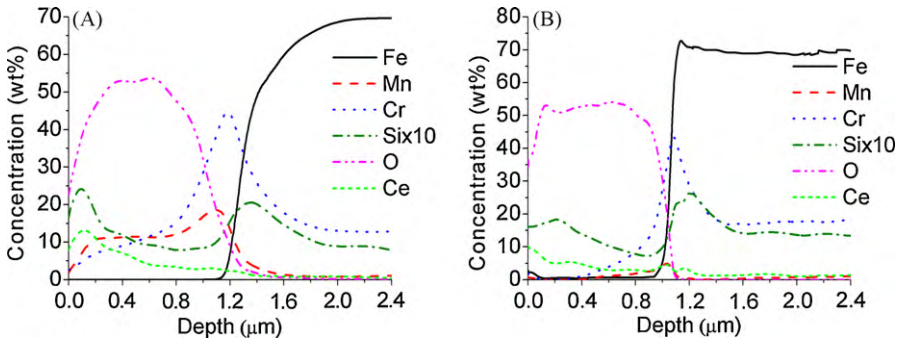

Fig. 3. GD-OES of (A) CeO_2 and (B) Au/CeO_2 monoliths.

Table 2
Textural properties of coated monoliths and powder catalysts.

	CeO_2		Au/CeO_2	
	Monolith	Powder	Monolith	Powder
Catalyst deposited (mg)	96.8	–	103.4	–
Adherence (%)	99.0	–	98.9	–
S_{BET} (m^2 monolith^{-1})	10	–	13	–
S_{BET} (m^2 g catal^{-1})	100	118	121	125
Pore volume (cm^3 monolith^{-1})	0.014	–	0.011	
Pore volume (cm^3 g catal^{-1})	0.130	0.039	0.113	0.049
Pore diameter (Å)	41	27	53	29

thickness of the catalytic layer, ca. 1.05 μm, is calculated according to a procedure previously reported [4]. It takes into account the amount of coating (ca. 100 mg), the total surface area of the metallic sheets used to built a monolith (240 cm^2) and the density of the coating, calculated from ceria bulk density and the pore volume measured by N_2 adsorption–desorption isotherms.

The AISI 304 stainless steel deposited catalytic layers, CeO_2 and Au/CeO_2, are highly homogeneous as observed by SEM micrographs (figures not shown), being noteworthy the absence of cracks within the catalytic layers whose composition is confirmed by EDX. In the gold-containing catalysts the presence agglomerations of gold clusters, as big as 800 nm, are detected.

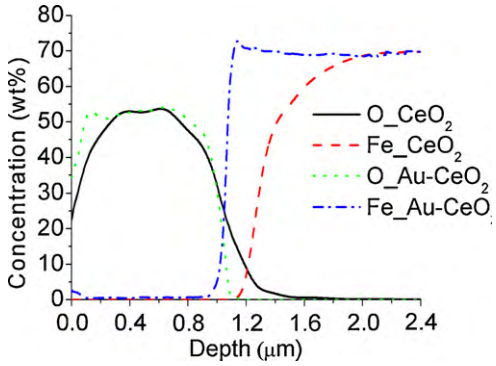

Fig. 4. Oxygen and iron GD-OES analysis of CeO_2 and Au/CeO_2 monolithic catalysts.

GD-OES allows estimate the oxide scale thickness estimated through oxygen in-depth profile. The average thickness is ca. 1 μm for CeO_2 and Au/CeO_2 monoliths, Fig. 3. This value closely agrees with the calculated theoretical average thickness. The oxide layer upon catalyst deposition is ~300 nm thicker than the original oxide scale, however, there is not a sharp interface between the catalyst and the oxide scale but cerium penetrates deep in the oxide layer reaching the oxide–alloy interface, although cerium concentration

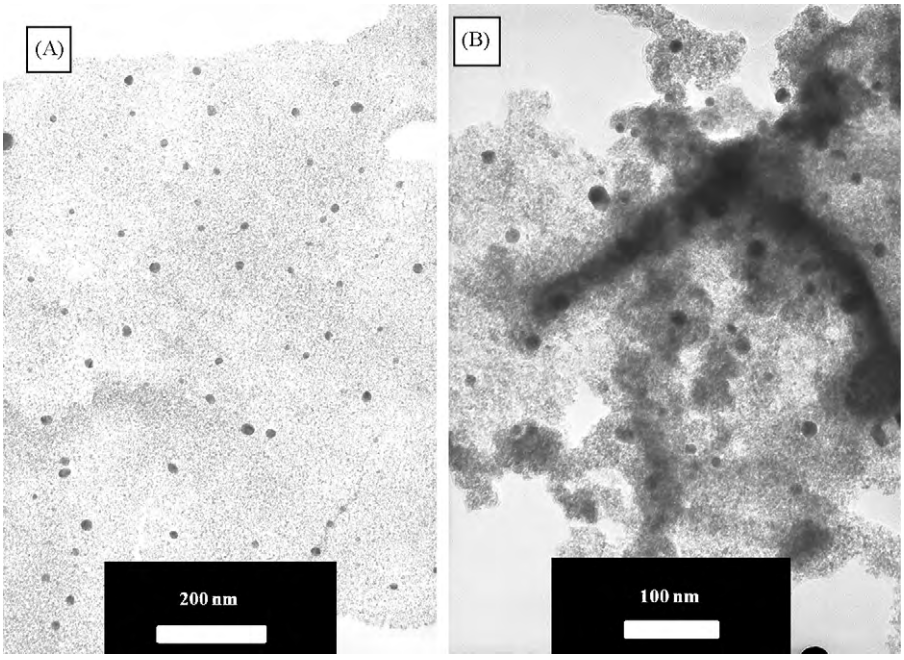

Fig. 5. TEM micrographs of powder catalysts extracted from the Au/CeO_2 monolith.

is higher in the outermost part of the oxide layer. Moreover, a modification of the composition and distribution of the oxide scale with respect to that of the uncoated monolith is observed.

The GD-OES profiles of the CeO_2-coated monolith (Fig. 3A) and Au/CeO_2 monolith (Fig. 3B) are rather similar. The main difference are the iron oxidation and the diffusion from the alloy bulk to the surface in the case of Au/CeO_2 monolith. Although the thickness of the oxidation scale calculated from the oxygen concentration is almost the same in both CeO_2 and Au/CeO_2 samples (around 1.0 μm), the chromium depletion is hardly observed in the gold catalyst. Therefore, the bulk concentration of iron is reached at around 2.0 μm in CeO_2 monolith and at 1.3 μm in Au/CeO_2 monolith, Fig. 4.

The average gold particle size is 11 nm although the particle size distribution is quite heterogeneous; this value is estimated from TEM images of catalyst powders extracted from the Au/CeO_2 monolith (Fig. 5).

3.3. Powder catalysts

Textural properties of the catalysts are reported in Table 2. The isotherms correspond to typical mesoporous materials with average pore sizes of ca. 27 Å. The Au/CeO_2 catalyst has higher S_{BET} and pore diameter than CeO_2 catalyst. The expansion of the mesoporous structure of the support since the introduction of gold particles has been early reported [6,7,22].

The XRD patterns of the solids (Fig. 6) show diffraction lines corresponding to cerianite (CeO_2). The ceria crystallite size was calculated to be 6.0 and 6.3 nm for CeO_2 and Au/CeO_2, respectively. In addition, Au/CeO_2 shows peaks assigned to metallic gold with an average crystallite size of 21 nm. In this sample, the average gold particle size determined from TEM micrographs was 28 nm (Fig. 7) and the gold loading measured by XRF was 0.88 wt.%, very close to the intended content.

3.4. Catalytic test

The pre-treated AISI 304 steel monolith does not show activity in the CO oxidation at temperatures below 300 °C. CO conversion started at 400 °C being below 5% at 500 °C (not shown).

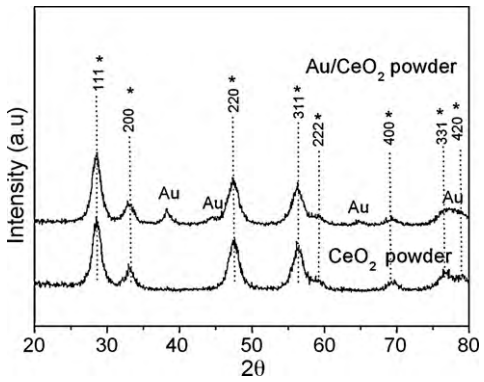

Fig. 6. XRD patterns of the powder catalysts. Symbols: (*) CeO_2 and (Au) gold.

CO light-off curves of the prepared monolithic and powder catalysts are shown in Fig. 8. The catalytic activity of the ceria catalyst is lower than those obtained for the support deposited on the monolithic substrate. The CeO_2 powder reaches 40% CO conversion at 300 °C, while the ceria-coated monolith shows total conversion at this temperature. The higher catalytic activity of the monolithic device may indicate the influence of the oxide scale form on AISI 304 stainless steel on ceria catalytic activity. This must be related to the presence of transition metal atoms coming from the oxide scale of the stainless steel treated surface [4,7]. The metal content of the stainless steel wastes used for preparing ceramic foams has a positive influence in the activity of gold-supported catalysts coated on these ceramic foams [7]. This behaviour, also reported in other stainless steel supported gold catalysts [4] put in evidence that transition metal atoms present in the oxide scale are active centers for the CO oxidation reaction.

As expected the presence of gold highly enhances the catalytic activity of the catalysts in the CO oxidation reaction. Complete CO conversion is achieved at low temperatures (ca. 110 °C) in both powder and monolithic device. The CO oxidation activity is mainly due to gold sites, therefore, differences between the activities obtained for the powder and monolithic catalysts is hardly observed.

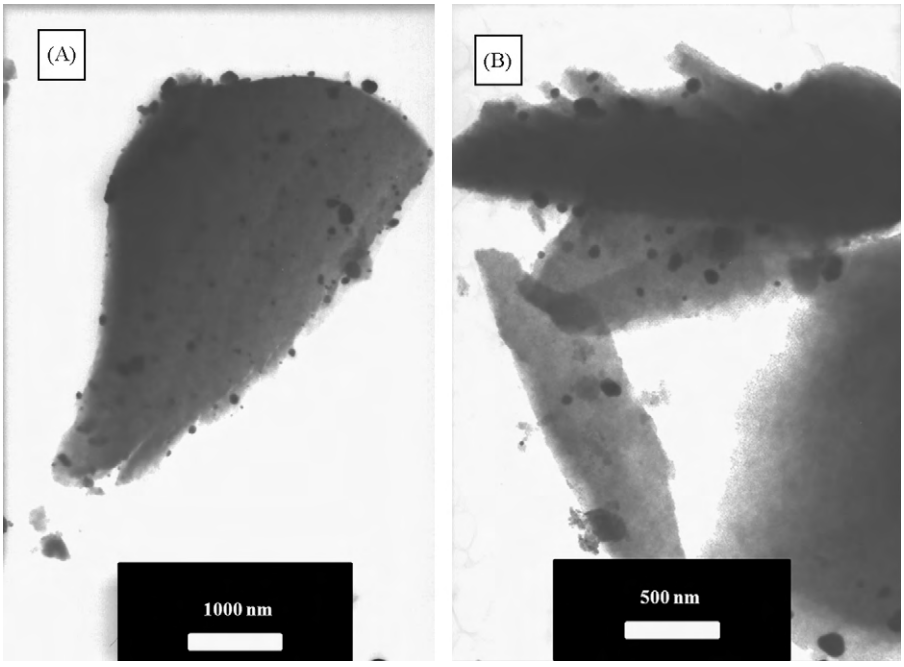

Fig. 7. TEM micrographs of Au/CeO_2 powder catalysts.

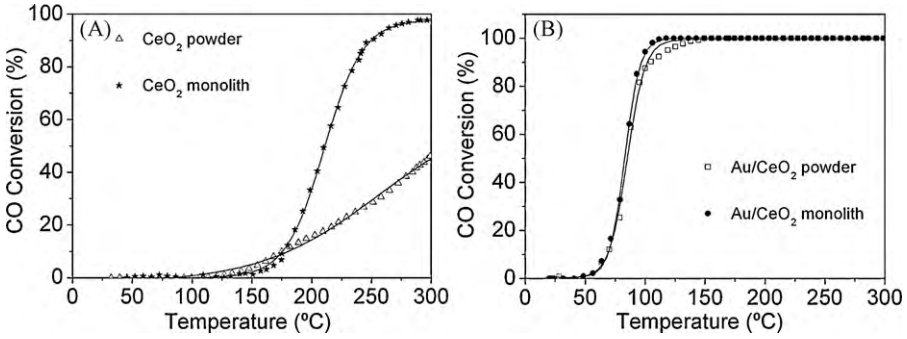

Fig. 8. Conversion of CO using powder and monolithic catalysts: (A) CeO_2 and (B) Au/CeO_2 catalysts.

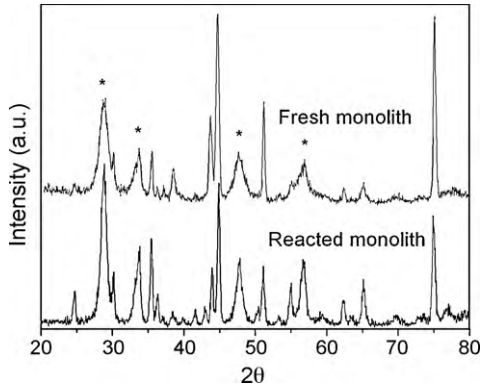

Fig. 9. XRD pattern of fresh and reacted Au/CeO_2 monoliths. Symbol: (*) CeO_2.

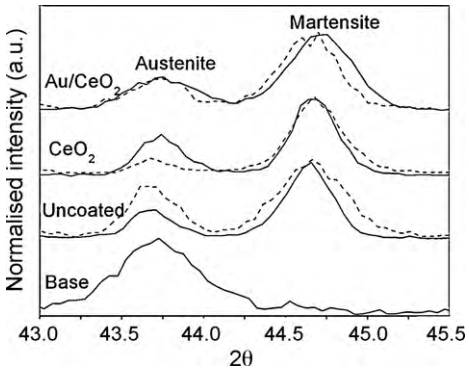

Fig. 10. Normalised XRD austenite/martensite ratio in monolithic catalysts. Fresh monoliths (solid lines) and reacted monoliths (dash lines).

3.5. Reacted catalysts

3.5.1. Monolithic devices

Crystalline phases remains unchanged in the reacted monolithic catalysts as evidenced by XRD patterns; however, changes in the relative intensity of characteristic diffraction peaks of existing crystalline phases with respect to the fresh catalysts are observed. Diffraction lines corresponding to cerianite phase increase their intensity in the reacted monoliths, becoming the most intense diffraction lines in the XRD pattern of the reacted Au/CeO_2 monolith (Fig. 9). Besides this, the intensity of the diffraction lines responsible for the austenite/martensite ratio is modified after reaction (Fig. 10). This ratio increases, after reaction, for the uncoated monolith. This indicates that the recovery of the chromium-depleted region of the alloy remains constant for Au/CeO_2 and decrease for CeO_2 ones resulting in turn in widening of the chromium-depleted region of the alloy. On the other hand, the average crystallite size of ceria and gold, estimated using the Scherrer equation, does not appreciably change with respect to those measured for fresh monoliths (ceria. 13 and 7 nm for CeO_2 and Au/CeO_2, respectively; gold: 19 nm).

The GD-OES results show that the oxide layer of the monoliths grows after reaction (Fig. 11). The oxide scale thickness, calculated from the oxygen concentration, was 1.8 and 1.3 μm for the ceria and gold/ceria reacted monoliths, respectively. This thickness growth is responsible for the intensity increase of the ceria phase in the XRD patterns. Moreover, a modification of the oxide scale profiles is produced after reaction. Cerium migrates to the inner part of the oxide scale; silicon is detected in the outer surface and chromium and manganese distribution in the oxide scale changes. In the case of the gold catalysts, iron continues being present in the external surface layer.

The average gold particle size calculated from TEM analysis of the powder catalyst extracted from the reacted Au/CeO_2 monolith was 16 nm.

3.5.2. Powder catalysts

The XRD patterns of the reacted catalysts are shown in Fig. 12. As for the fresh catalysts, only peaks due to cerianite and metallic gold are present. From the Scherrer equation, ceria crystallite size was calculated to be 6.1 and 6.0 nm for CeO_2 and Au/CeO_2, respectively.

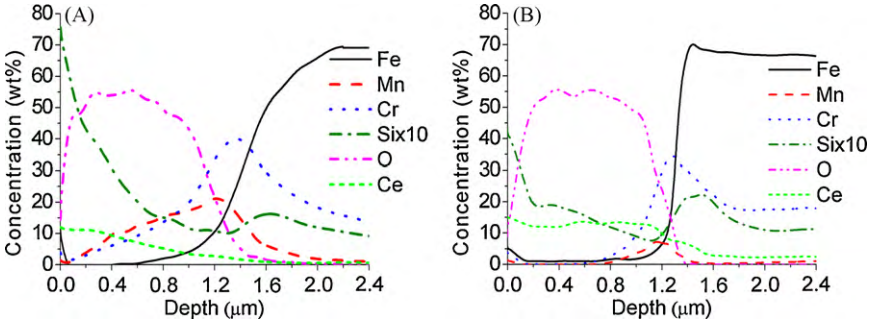

Fig. 11. GD-OES results of the monoliths after reaction coated by (A) CeO_2 and (B) Au/CeO_2.

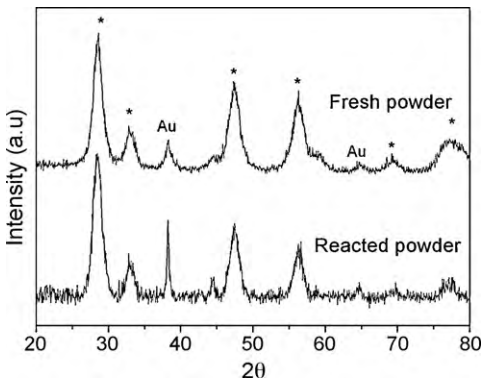

Fig. 12. XRD pattern of fresh and reacted Au/CeO_2 powders. Symbols: (*) CeO_2 and (Au) gold.

Gold particles are estimated to have an average crystallite size of 32 nm while the average metal particles size determined from TEM micrographs was 35 nm (not shown).

4. Discussion

Success of metallic structured reactors depends on the formation of homogeneous, uniform and well-adhered catalytic layers on the metallic surface. As these surfaces show low adherence of the ceramic materials often used as catalysts, a suitable treatment of the metallic substrate is required to improve this adherence. In the case of AISI 304 austenitic stainless steels, a thermal treatment under synthetic air at 900 °C for 1 h is suitable [3]. In these conditions, 0.7 μm of an oxide layer composed mainly of manganese and chromium oxides ($Mn_{1+x}Cr_{2-x}O_{4-x}$, Cr_2O_3) is developed. A continuous Si interface is also formed between the oxide scale and the metallic alloy. This silicon-containing layer affects the diffusion of Cr and Fe from the alloy to the oxide scale and acts as a diffusion barrier for the mobility of cations during thermal oxidation of stainless steels [24,25]. The thickness and composition of the oxide scale depends on the alloying elements as well as the temperature, time and atmosphere of pretreatment [6,22]. Therefore, the thermal pretreatment must be carefully selected for every metallic substrate to allow appropriate oxidation of the alloy elements to develop a resistant, rough and homogeneous oxide layer, which could improve further anchoring of the catalytic phase.

In the present work, colloidal solutions with the adequate composition and rheological properties were selected for washcoating the catalyst onto the metallic monolith. For these processes only colloidal dispersions were used, even in the case of Au/CeO_2 catalyst, allowing good reproducibility and a minor consumption of time. Upon drying and calcination a homogenous and well-adhered catalytic layer is obtained. The measured thickness of such layer, which corresponds with the theoretical value, is similar for CeO_2 and Au/CeO_2 catalysts, 1.0 μm. As the metallic substrate oxide scale before deposition is 0.7 μm, the measured thickness means that the catalytic layer settles covering the empty spaces left by the polyhedral crystals forming the scale. Moreover, GD-OES reveals that elements from the catalytic layer, cerium in our case, penetrate through the oxide scale reaching the alloy. Besides this, an alteration of the composition of the oxide scale is also produced, being detected diffusion of silicon, chromium and manganese to the surface. The presence of such metallic atoms in the catalytic layer coming from the oxide scale enhances the catalytic activity of bare CeO_2 powder as can be seen in Fig. 8. We have previously reported these observations for other systems [4,6,7]. Even more, it is well known that stainless steel reactors may present wall effects in many catalytic reactions such as 1,3 butadiene oxidation [27], selective oxidation of cyclohexane [28], oxidative coupling of methane [29], olefins oxidation in supercritical CO_2 [30], steam cracking and steam reforming of waste cooking oil [31], among others. In these papers, it is demonstrated that the surface of the stainless steel reactor has an effect on the reaction and plays an active role in some surface reactions, being in general, beneficial to total oxidation ones.

In our case, the main difference observed on washcoating CeO_2 or Au/CeO_2 resides in the oxidation and diffusion of bulk iron to the oxide scale for the gold-containing catalyst, Fig. 4. This effect may have catalytic implications. In a recent study we have reported the

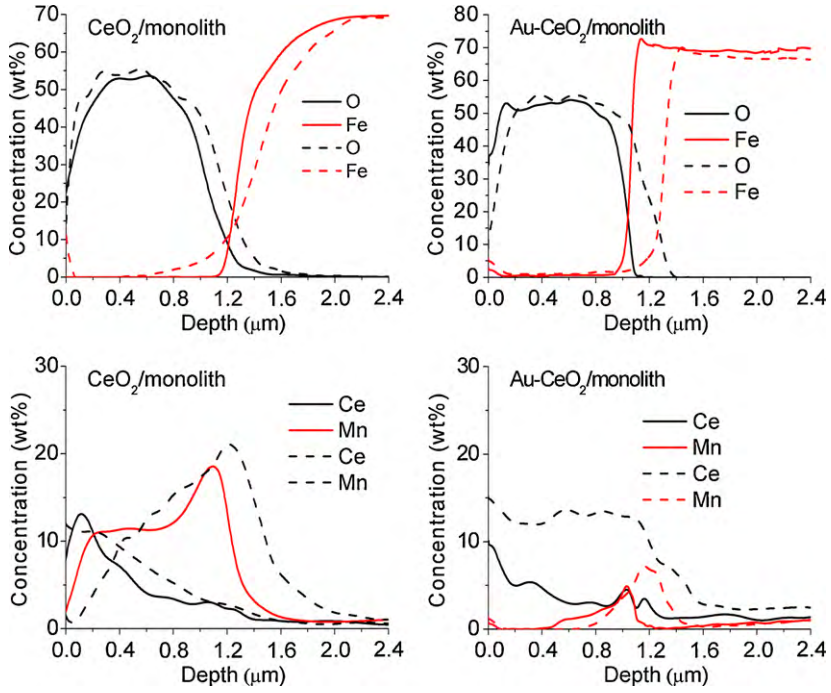

Fig. 13. GD-OES analysis of the distribution of O and Fe (top figures) and Ce and Mn (bottom figures) on fresh (solid lines) and reacted (dash lines) monolithic devices.

high activity of $Au/FeO_x/CeO_2$ catalysts for CO total oxidation and COPROX reactions [32,33]. The Au^{n+}/Au^0, Ce^{4+}/Ce^{3+} and Fe^{3+}/Fe^{2+} redox couples would be responsible of such high activity. This observation, together with the reported possibility of introducing Fe in the CeO_2 network resulting in a Ce–Fe oxide solid solution [33], could explain the iron migration. The relatively high Au loading and the reduced amount of iron in the outermost part of the oxide layer present in the Au/CeO_2 catalysts prevents the observation of significant differences between powder and monolithic catalysts in the oxidation of CO.

On the other hand, the diffusion and mixture of elements coming from the catalyst and the oxide scale could result in a modification of the textural properties, crystalline phases, particle sizes and catalytic properties of the catalysts compared to those of the powder ones. No differences in the crystalline phases or gold particle sizes are detected, although CeO_2 crystalline domain sizes are significantly higher in the monolithic device.

The characterization of the reacted catalysts evidences their evolution under reaction conditions. GD-OES results reveal a growth of the oxide layer thickness and a change in the metallic atoms distribution of the oxide scale. As an example, the in-depth composition in O, Fe, Ce and Mn for the fresh and reacted CeO_2 and Au/CeO_2 monolithic catalysts are depicted in Fig. 13. Although the thickness of the scale has increased, cerium ions are present in the whole scale and iron diffuses from the alloy bulk to the oxide scale while manganese concentration in the outermost layer decreases.

All these observations confirm the oxidation of the alloy and the migration of the metallic cations across the scale. As a result the oxide scale has increased their thickness after reaction. The intensity of cerianite diffraction lines is relatively higher than the intensity of diffraction lines corresponding to the alloy phases indicating the thickness increase (Fig. 9). Moreover, changes in the diffraction line intensity fcc/bcc ratio are produced (Fig. 10). The stainless steel oxide scale formation proceeds by short-circuit diffusion processes. In this processes, the alloy surface layers changes their composition as a result of outward cation diffusion resulting in the austenite to martensite transformation [3]. For the reacted ceria monolith the bcc layer is thicker than before reaction. As stated above cerium ions hinders the outward diffusion of cations and only inwards oxide diffusion is responsible for the thickness increase, the selective oxidation of chromium and manganese in the alloy surface layers results in an increase of the bcc layer thickness [4,6,7]. On the other hand, gold particles nucleate on surface oxygen vacancies of ceria [16] and therefore might migrate together with cerium to the alloy/scale interface. Therefore, at the interface the redox Au^{n+}/Au^0, Ce^{4+}/Ce^{3+} and Fe^{3+}/Fe^{2+} pairs [32,33] allow the outward diffusion of cations and the inwards diffusion of anions resulting in thicker oxide scales but thin bcc layers as evidenced by the relative intensity of the diffraction lines of these phases, Fig. 10, and the sharp edge in iron concentration observed in the GD-OES profile, Fig. 11. The beneficial effect of REE elements, cerium among them, results in an oxidation behaviour following Wagner's law, the oxidation rate decrease with the square root of the oxidation time. This behaviour allows suggesting the composition and thickness of the oxide layer will hardly change for successive reaction cycles.

We cannot observe, using XRD, new crystalline phases upon reaction or modifications of the average crystallite sizes of gold or ceria phases for the monolithic catalyst. However, the average gold crystallite size increased after reaction for the powder sample (from 20 to 30 nm). It is well know that gold crystallite size is a function of temperature and reaction atmosphere [34]. Usually, gold particles sinterizes upon reaction, although it gold redispersion under reaction conditions can also occur [16,35]. The different behaviours of gold particle sizes for powder and monolithic catalysts evidence a different gold surface dynamics in Au/CeO_2 catalysts when supported on the metallic surface. This is probably due to the presence of metallic cations coming from the metal surface in the catalysts, and/or changes in the diffusion and transport phenomena of the reactants in the catalytic layer as can be observed in Fig. 8. In this sense, it is recently demonstrated that redox processes involving surface hydroxyl groups, gold atoms, and gas-phase CO molecules play a determinant role in the surface dynamics of gold particles, which in turns results after reaction in changes in the gold particle size [16]. The presence of metallic cations with active redox couples, such as Fe, could also modify the gold surface dynamics resulting in different Au particle sizes.

5. Conclusions

This work presents evidences for the modification of the formulation for CeO_2 and Au/CeO_2 catalysts deposited on stainless steel surfaces. The diffusion of metallic cations present in the oxide scale to the catalytic layer and the diffusion of elements from the catalyst coating to the oxide scale alters the catalyst formulation, resulting in a modification of the oxide scale/alloy and oxide coating/alloy interfaces. Moreover, the deposition process favours the oxidation of the alloy. The extension and nature of these modifications depends on the catalysts nature. Thus, in both catalytic devices, ceria diffuses through the oxide scale, reaching the alloy/oxide scale interface, and manganese, iron, chromium and silicon are detected in the catalytic layer. For Au/CeO_2 monolith a migration of iron from the alloy with the formation of an iron–rich layer is observed by GD-OES. Characterization of the monolithic devices after CO oxidation also shows the modification of the catalytic layer after reaction. These alterations in the catalytic layer have influence in the catalytic properties, resulting in the enhancement of the oxidation performances of ceria catalysts and modifying the surface dynamics of gold in the Au/CeO_2 ones.

Acknowledgments

The financial support for this work has been obtained from Spanish Ministerio de Ciencia e Innovación (ENE2009-14522-C05-01 and MAT2006-12386-C05-01), Junta de Andalucía (P06-TEP-01965) and co-financed by FEDER funds from European Union. L.M. Martínez T thanks the Alßan program for the fellowship awarded (E04D046878CO).

References

[1] E. Tronconi, G. Groppi, Chem. Eng. Sci. 55 (2000) 6021.
[2] P. Avila, M. Montes, E.E. Miro, Chem. Eng. J. 109 (2005) 11.
[3] L.M. Martínez T, O. Sanz, M.I. Domínguez, M.A. Centeno, J.A. Odriozola, Chem. Eng. J. 148 (2009) 191.
[4] L.M. Martínez T, D.M. Frías, M.A. Centeno, A. Paúl, M. Montes, J.A. Odriozola, Chem. Eng. J. 136 (2008) 390.
[5] D.M. Frias, S. Nousir, I. Barrio, M. Montes, L.M. Martínez T, M.A. Centeno, J.A. Odriozola, Appl. Catal. A: Gen. 325 (2007) 205.
[6] L.M. Martínez T, M.I. Domínguez, N. Sanabria, W.Y. Hernández, S. Moreno, R. Molina, J.A. Odriozola, M.A. Centeno, Appl. Catal. A: Gen. 364 (2009) 166.
[7] M.I. Domínguez, M. Sánchez, M.A. Centeno, M. Montes, J.A. Odriozola, Appl. Catal. A 302 (2006) 96.
[8] M.J. Capitan, A. Paul, J.L. Pastol, J.A. Odrizola, Oxid. Metal 52 (1999) 447.
[9] S. Roure, F. Czerwinski, A. Petric, Oxid. Metal 42 (1994) 75.
[10] R. Thanneeru, S. Patil, S. Deshpande, S. Seal, Acta Mater. 55 (2007) 3457.
[11] A. Paúl, S. Elmrabet, F.J. Ager, J.A. Odriozola, Surf. Int. Anal. 30 (2000) 176.
[12] P. Papaiacovou, R.J. Hussey, D.F. Mitchell, M.J. Graham, Corros. Sci. 30 (1990) 451.
[13] A. Nazeri, P.P. Trzaskoma, D. Bauer, J. Sol-Gel Sci. Technol. 10 (1997) 317.
[14] G.C. Bond, D.T. Thompson, Catal. Rev. Sci. Eng. 41 (1999) 319.
[15] M. Haruta, N. Yamada, T. Kobayashi, S. Iijima, J. Catal. 115 (1989) 301.
[16] F. Romero-Sarria, L.M. Martinez T, M.A. Centeno, J.A. Odriozola, J. Phys. Chem. C 111 (2007) 14469.
[17] F. Romero-Sarria, A. Penkova, L.M. Martínez, M.A. Centeno, K. Hadjiivanov, J.A. Odriozola, Appl. Catal. B 84 (2008) 119.
[18] M.A. Centeno, C. Portales, I. Carrizosa, J.A. Odriozola, Catal. Lett. 102 (2005) 289.
[19] M.A. Centeno, M. Paulis, M. Montes, J.A. Odriozola, Appl. Catal. B 61 (2005) 177.
[20] M.A. Centeno, M. Paulis, M. Montes, J.A. Odriozola, Appl. Catal. A 234 (2002) 65.

[21] M.A. Centeno, K. Hadjiivanov, T. Venkov, H. Klimev, J.A. Odriozola, J. Mol. Catal. A: Chem. 252 (2006) 142.
[22] Z. Kònya, V.F. Puntes, J. Kiricsi, J. Zhu, J.W. Ager, M.K. Ko, H. Frei, P. Alivisatos, G.A. Somorjai, Chem. Mater. 15 (2003) 1242.
[23] C.K. Costello, J.H. Yang, H.Y. Law, Y. Wang, J.N. Lin, L.D. Marks, M.D. Kung, H.H. Kung, Appl. Catal. A 243 (2003) 15.
[24] A. Paúl, S. ElmRabet, F.J. Ager, J.A. Odriozola, M.A. Respaldiza, M.F. da Silva, J.C. Soares, Oxid. Met. 57 (2002) 33.
[25] T. Horita, H. Kishimoto, K. Yamaji, M.E. Brito, H. Yokokawa, Y. Baba, K. Ogasawara, H. Kameda, Y. Matsuzaki, S. Yamashita, N. Yasuda, T. Uehara, Solid State Ionics 179 (2008) 2216.
[26] J.M. Zamaro, M.A. Ulla, E.E. Miró, Catal. Today 107–108 (2005) 86.
[27] P.L. Mills, J.F. Nicole, Ind. Eng. Chem. Res. 44 (2005) 6453.
[28] J. Haoa, H. Chenga, H. Wanga, S. Caia, F. Zhao, J. Mol. Catal. 271 (2007) 42.
[29] X.Q. Qiu, Q.M. Zhu, N.B. Wong, K.C. Tin, J. Chem. Tech. Biotechnol. 65 (1996) 380.
[30] F. Loeker, W. Leitner, Chem. Eur. J. 6 (2000) 2011.
[31] J. Gornay, L. Coniglio, F. Billaud, G. Wild, Energy Fuels 23 (2009) 5663.
[32] A. Penkova, K. Chakarova, O.H. Laguna, K. Hadjiivanov, F. Romero-Sarria, M.A. Centeno, J.A. Odriozola, Catal. Commun. 10 (2009) 1196.
[33] O.H. Laguna, M.A. Centeno, G. Arzamendi, L.M. Gandía, F. Romero-Sarria, J.A. Odriozola, Catal. Today, 2010, in press, doi:10.1016/j.cattod.2010.04.011.
[34] R. Zanella, C. Louis, Catal. Today 107–108 (2005) 768.
[35] A. Goguet, C. Hardacre, I. Harvey, K. Narasimharao, Y. Saih, J. Sa, J. Am. Chem. Soc. 131 (2009) 6973.